Search for *C*-even states decaying to $D_s^\pm D_s^{*\mp}$ with masses between 4.08 and 4.32 GeV/c^2

M. Ablikim *et al.*[*]

(BESIII Collaboration)

Six *C*-even states, denoted as *X*, with quantum numbers $J^{PC} = 0^{-+}$, $1^{\pm+}$, or $2^{\pm+}$, are searched for via the $e^+e^- \to \gamma D_s^\pm D_s^{*\mp}$ process using (1667.39 ± 8.84) pb^{-1} of e^+e^- collision data collected with the BESIII detector operating at the BEPCII storage ring at center-of-mass energy of $\sqrt{s} = (4681.92 \pm 0.30)$ MeV. No statistically significant signal is observed in the mass range from 4.08 GeV/c^2 to 4.32 GeV/c^2. The upper limits of $\sigma[e^+e^- \to \gamma X] \cdot \mathcal{B}[X \to D_s^\pm D_s^{*\mp}]$ at a 90% confidence level are determined.

I. INTRODUCTION

The charmonium(like) system is a good laboratory for studying the nonperturbative behavior of quantum chromodynamics (QCD). Over the past two decades, many new resonant structures have been discovered that cannot be explained by a simple mesonic ($q\bar{q}$) or baryonic (qqq) configurations. This has sparked significant experimental and theoretical interest.

Charmonium states with mass above the open-charm threshold are expected to decay dominantly into open-charm final states [1–3]. In Ref. [4], the masses and total widths of the $\chi_{c2}(3P), \chi_{c1}(3P)$, and $\eta_{c2}(2D)$ are calculated using either the nonrelativistic potential model or the relativized Godfrey-Isgur model [5]. The open-charm strong decay widths are estimated by using harmonic oscillator wave functions and the $^3P_0$ decay model. These states are predicted to have sizeable decay widths to the $D_s^\pm D_s^{*\mp}$ final state, as listed in Table I. However, none of these states have been observed experimentally so far. In an amplitude analysis of the $B^+ \to J/\psi\phi K^+$ decay, a 1^{++} state was observed in the $\phi J/\psi$ final state [6–8], with an average mass of 4286^{+8}_{-9} MeV/c^2, which is close to the predicted mass of the $\chi_{c1}(3P)$. Its assignment as a $\chi_{c1}(3P)$ state requires further confirmation.

In the hybrid meson ($q\bar{q}g$) configuration, several states are predicted by lattice QCD [10,11]. The strong decay widths of these hybrid states are computed based on the constituent gluon model [12]. The $D_s^\pm D_s^{*\mp}$ mode is expected to be the leading decay channel for the $X(4217)$ with $J^{PC} = 1^{-+}$ and the $X(4279)$ with $J^{PC} = 0^{-+}$, where the numbers in the brackets denote the theoretical masses of the hybrid states. The resonant parameters of the two states are summarized in Table I.

The authors of Ref. [9] provide a whole spectrum of heavy-antiheavy hadronic molecules by solving the Bethe-Salpeter equation. A virtual state, referred to as the $X(4080)$ in this paper, with a mass close to the $D_s^\pm D_s^{*\mp}$ threshold, is expected to decay predominantly to $D_s^\pm D_s^{*\mp}$. Its quantum numbers are $J^{PC} = 1^{++}$ and its total width is assumed to be 5 MeV. Many structures from experiments with masses near the thresholds of a pair of open-charm mesons are reported, such as the $X(3872)$ [13], $Z_c(3900)^\pm$ [14–16], $Z_c(4020)^\pm$ [17,18], and $Z_{cs}(3985)$ [19,20], which are near the thresholds of $D^0\bar{D}^{*0}$, $D\bar{D}^*$, $D^*\bar{D}^*$, and $D_s^{(*)}\bar{D}^{(*)}$, respectively. Motivated by both experimental observations and theoretical calculations, searching for the structure near the threshold of $D_s^\pm D_s^{*\mp}$ is crucial.

It has been demonstrated that *C*-even states can be produced in e^+e^- collisions accompanied by photon emission. For instance, the $e^+e^- \to \gamma X(3872)$ [21] and $\gamma\chi_{c1,2}(1P)$ [22] processes have been observed by the BESIII experiment. In this paper, a study of $e^+e^- \to \gamma D_s^\pm D_s^{*\mp}$ is presented to search for the aforementioned *C*-even structures. Throughout this paper, the charge conjugated mode is implied. This analysis utilizes a data sample collected at center-of-mass energy $\sqrt{s} = (4681.92 \pm 0.08 \pm 0.29)$ MeV with an integrated luminosity of $(1667.39 \pm 0.21 \pm 8.84)$ pb^{-1} [23], where the first and second uncertainties are statistical and systematic, respectively. The D_s^* meson is reconstructed using its radiative decay into the γD_s final state. The D_s meson is reconstructed with its decay modes $D_s \to K^+K^-\pi$ and

---

TABLE I.   Predicted masses (M), total widths (Γ), partial widths ($\Gamma_{D_s^\pm D_s^{*\mp}}$), and quantum numbers of the six C-even states.

State	M (MeV/c^2)	Γ (MeV)	$\Gamma_{D_s^\pm D_s^{*\mp}}$ (MeV)	J^{PC}
$\eta_{c2}(2D)$ [4]	4158	111	18	2^{-+}
$\chi_{c1}(3P)$ [4]	4271	39	9.7	1^{++}
$\chi_{c2}(3P)$ [4]	4317	66	11	2^{++}
$X(4080)$ [9]	4082.55	5	$\cdots$	1^{++}
$X(4217)$ [10–12]	4217	6	6	1^{-+}
$X(4279)$ [10–12]	4279	110	34	0^{-+}

$K_S^0 K$, with $K_S^0 \to \pi^+\pi^-$. These two decay modes of the D_s are combined into four decay chains (DCs):

DC-I: $D_s^+ D_s^- \to (K^+ K^- \pi^+)(K^+ K^- \pi^-)$,
DC-II: $D_s^+ D_s^- \to (K^+ K^- \pi^+)(K_S^0 K^-)$,
DC-III: $D_s^+ D_s^- \to (K_S^0 K^+)(K^+ K^- \pi^-)$, and
DC-IV: $D_s^+ D_s^- \to (K_S^0 K^+)(K_S^0 K^-)$.

II. BESIII DETECTOR AND MONTE CARLO SIMULATION

The BESIII detector [24] records symmetric e^+e^- collisions provided by the BEPCII storage ring [25], which operates with a peak luminosity of 1×10^{33} cm^{-2} s^{-1} in the center-of-mass energy range from 2.0 GeV to 4.95 GeV [26]. The cylindrical core of the BESIII detector covers 93% of the full solid angle and consists of a helium-based multilayer drift chamber (MDC), a plastic scintillator time-of-flight system (TOF), and a CsI(Tl) electromagnetic calorimeter (EMC), which are all enclosed in a superconducting solenoidal magnet providing a 1.0 T magnetic field. The solenoid is supported by an octagonal flux-return yoke with resistive plate counter muon identification modules interleaved with steel. The charged-particle momentum resolution at 1 GeV/c is 0.5%, and the dE/dx resolution is 6% for electrons from Bhabha scattering. The EMC measures photon energies with a resolution of 2.5% (5%) at 1 GeV in the barrel (end cap) region. The time resolution in the TOF barrel region is 68 ps, while that in the end cap region is 60 ps [27–29].

Simulated events produced with a GEANT4-based [30] Monte Carlo (MC) package are used to determine detection efficiencies and to estimate backgrounds. This MC package includes the geometric description of the BESIII detector and the detector response. The simulation models the beam energy spread and initial state radiation (ISR) in the e^+e^- annihilations with the generator KKMC [31,32]. The generic MC samples include the production of open-charm processes, the ISR production of vector charmonium(like) states, and the continuum processes implemented in KKMC [31,32]. The known decay modes are modeled with EVTGEN [33,34] using branching fractions taken from the Particle Data Group (PDG) [35], and the remaining unknown charmonium decays are modeled with LUNDCHARM [36,37]. Final state radiation for charged final state particles is incorporated using the PHOTOS package [38].

The signal processes $e^+e^- \to \gamma X$, $X \to D_s^\pm D_s^{*\mp}$ and their subsequent decays are modeled with EVTGEN [33,34]. The $D_s \to K^+ K^- \pi$ decay is generated according to the amplitude models reported in Refs. [39,40]. Two groups of samples are generated for the signal processes, Group-I and Group-II. Group-I is produced with the predicted masses and widths of the X as listed in Table I, while Group-II is with the masses ranging from 4080 MeV/c^2 to 4320 MeV/c^2 in steps of 40 MeV/c^2 and widths varying from a set of values; 5 MeV, 10 MeV, 20 MeV, 50 MeV, 80 MeV, and 100 MeV. The quantum numbers J^{PC} of X are listed in Table I. In the signal MC simulations of $e^+e^- \to \gamma X$, γX are assumed to generate from $\psi(4660)$, and $\psi(4660)$ is parametrized using a Briet-Wigner function with parameters taken from the PDG [35].

Additional MC samples of $e^+e^- \to (\gamma_{\rm ISR})D_s^{(*)\pm}D_s^{*\mp}$, $(\gamma_{\rm ISR})D_s^* D_{s0}^*(2317)$, and $(\gamma_{\rm ISR})D_s^{(*)}D_{s1}(2460)$ events are generated to estimate the background contamination. They are modeled using helicity-amplitude models or phase space in EVTGEN [33,34]. The production cross sections are taken from previous BESIII measurements [41–43].

III. EVENT SELECTION AND BACKGROUND STUDY

A full reconstruction method is used to reconstruct the signal process $\gamma D_s^\pm D_s^{*\mp}(\to \gamma D_s^\mp)$, $D_s \to K^+ K^- \pi$ or $K_S^0(\to \pi^+\pi^-)K$. Charged tracks detected in the MDC are required to be within a polar angle (θ) range of $|\cos\theta| < 0.93$, where θ is defined with respect to the symmetry axis of the MDC (defined as the z-axis). For charged tracks not originating from K_S^0 decays, the distance of the closest approach to the interaction point (IP) must be less than 10 cm along the z-axis (V_z), and less than 1 cm in the transverse plane (V_{xy}). Particle identification (PID) for charged tracks combines measurements of the energy deposited (dE/dx) in the MDC and the flight time in the TOF to form a likelihood for each hadron hypothesis. Tracks are identified as kaons (pions) when the kaon (pion) hypothesis has larger probability. Tracks without PID information are rejected.

Each K_S^0 candidate is reconstructed from two oppositely charged tracks satisfying $|V_z| < 20$ cm and $|\cos\theta| < 0.93$. The two charged tracks are assigned as $\pi^+\pi^-$ without

imposing PID criteria. They are constrained to originate from a common vertex and are required to have an invariant mass $(M_{\pi^+\pi^-})$ within the interval $(0.478, 0.518)$ GeV/c^2. The χ^2 of the vertex fit is required to be less than 100. A secondary vertex fit is performed to ensure that the K_S^0 momentum points back to the IP. The decay length of the K_S^0 candidate is required to be greater than twice the vertex resolution.

Photon candidates are identified using isolated showers not associated with charged tracks in the EMC. The deposited energy of each shower must be greater than 25 MeV in the barrel region ($|\cos\theta| < 0.8$) and greater than 50 MeV in the end cap regions ($0.86 < |\cos\theta| < 0.92$). The difference between the EMC time and the event collision time is required to be within $[0, 700]$ ns to suppress electronic noise and showers unrelated to the event.

The selected $K^\pm$, $\pi^\pm$, and K_S^0 candidates in the event are combined to reconstruct $D_s \to K^+K^-\pi$ or $D_s \to K_S^0 K$. The D_s candidates are kept if the invariant masses of the $K^+K^-\pi$ or $K_S^0 K$ systems, denoted as M_{D_s}, are within a ± 150 MeV/c^2 mass window around the nominal D_s mass. The $D_s^+D_s^-$ pairs are selected requiring that each $K^\pm$, $\pi^\pm$, and K_S^0 candidate is used in one $D_s^+D_s^-$ pair at most once. If there is more than one pair with the same DC in an event, the one with $(M_{D_s^+} + M_{D_s^-})/2$ closest to the nominal mass of the D_s meson [35] is chosen.

In addition to the $D_s^+D_s^-$ pair, each signal candidate is required to have at least two photons. A six-constraint (6C) kinematic fit is performed, where the four-momentum of the final state particles is constrained to that of the initial e^+e^- system and the masses of the reconstructed D_s^+ and D_s^- are constrained to their nominal masses. If more than two photons and (or) more than one $D_s^+D_s^-$ pair decaying in different DCs are found in an event, the combination with the minimum χ^2_{6C} is retained, and χ^2_{6C} is further required to be less than 200, where χ^2_{6C} is the χ^2 from the 6C kinematic fit. To study the background contributions from non-D_s processes, a four-constraint kinematic (4C) fit without the two D_s mass constraints is applied, and the four-momenta of the final state particles are computed using the momenta determined by the 4C kinematic fit.

To suppress background contributions from non-D_s processes, a D_s mass window of $|M_{D_s} - m_{D_s}| < 21$ MeV/c^2, which is about three times the mass resolution, is applied, where m_{D_s} is the nominal D_s mass. The two selected photon candidates and the two D_s mesons can form four combinations of γD_s. The one with invariant mass $(M_{\gamma D_s})$ closest to the nominal mass of the D_s^* is retained for further analysis. The invariant mass $M'_{\gamma D_s} = (M_{\gamma D_s} - M_{D_s} + m_{D_s})$ is required to be within the interval $(m_{D_s^*} \pm 27)$ MeV/c^2, where $m_{D_s^*}$ is the nominal $D_s^{*\pm}$ mass taken from the PDG [35]. The variable $M_{\gamma D_s}$ formed with the unused photon and D_s candidates is required to be

outside of this same mass window. The photon not from the D_s^* decay is labeled γ_1 and its recoil mass spectrum, $M_{\gamma_1}^{\text{rec}}$, is used to extract the signal yields. $M_{\gamma_1}^{\text{rec}}$ is calculated by $\sqrt{(E_{\text{cms}} - E_{\gamma_1})^2 - (\vec{P}_{\text{cms}} - \vec{P}_{\gamma_1})^2}$, where $(E_{\text{cms}}, \vec{P}_{\text{cms}})$ and $(E_{\gamma_1}, \vec{P}_{\gamma_1})$ are the four-momenta of the initial state [23] and γ_1, respectively. After imposing all the selection requirements, the dominant background processes are those that include one $D_s^+D_s^-$ pair in final states. The contributions from $e^+e^- \to (\gamma_{\text{ISR}})D_s^{(*)\pm}D_s^{*\mp}$, $(\gamma_{\text{ISR}})D_s^*D_{s0}^*(2317)$, and $(\gamma_{\text{ISR}})D_s^{(*)}D_{s1}(2460)$ events account for 76.9%, 4.4%, and 10.9% of the total backgrounds, respectively. The contributions from other background processes are less than 8%, and are found to be linearly distributed in the recoil mass spectrum of γ_1 based on the analysis of generic MC samples.

IV. SIGNAL YIELD EXTRACTION

The X signal yields are extracted using an unbinned maximum likelihood fit to the $M_{\gamma_1}^{\text{rec}}$ spectrum. The events from the four DCs are combined due to limited statistics. The fit probability density function (PDF) contains five components: signal (S), $e^+e^- \to (\gamma_{\text{ISR}})D_s^\pm D_s^{*\mp}$ background (B_1), $e^+e^- \to (\gamma_{\text{ISR}})D_s^{*\pm}D_s^{*\mp}$ background (B_2), $e^+e^- \to (\gamma_{\text{ISR}})D_s^{(*)}D_{sJ}$ background (B_3), and other remaining backgrounds (B_4). The function used in the fit is defined as

$$f_{\text{sum}} = N_{\text{sig}} \cdot S + \sum_{i=1}^{4} N_{\text{bkg}i} \cdot B_i,$$

where N_{sig} and $N_{\text{bkg}(1,2,3,4)}$ represent the numbers of signal events and background events, respectively. $N_{\text{bkg}(1,2,4)}$ are free parameters, and $N_{\text{bkg}3}$ is fixed according to BESIII measurement in the fit, $N_{\text{bkg}3} = 8.8 \pm 0.9$ [42,43], where the number of events and the uncertainty are from the cross section measurements.

The signal PDF is described by $S = BW(M_{\gamma_1}^{\text{rec}}; M, \Gamma) \otimes DG(m_1, \sigma_1, m_2, \sigma_2, f) \otimes G(\Delta m, \Delta \sigma)$, where BW stands for the Breit-Wigner function with mass M and width Γ fixed, DG is a double Gaussian function that describes the mass resolution and mass shift in the simulation, and G is a Gaussian function that accounts for the mass resolution difference between data and MC simulation. The parameters $m_1(m_2)$ and $\sigma_1(\sigma_2)$ represent the mean and standard deviation of the first (second) Gaussian function in the double Gaussian model, while f is the fraction of the first Gaussian component over the whole DG. To get the parameters of the double Gaussian function, the $M_{\gamma_1}^{\text{rec}} - M_{\gamma_1}^{\text{truth}}$ distribution from the signal MC samples is fitted, where $M_{\gamma_1}^{\text{truth}}$ is the recoil mass spectrum of the γ_1 distribution at generator level. The parameters of the
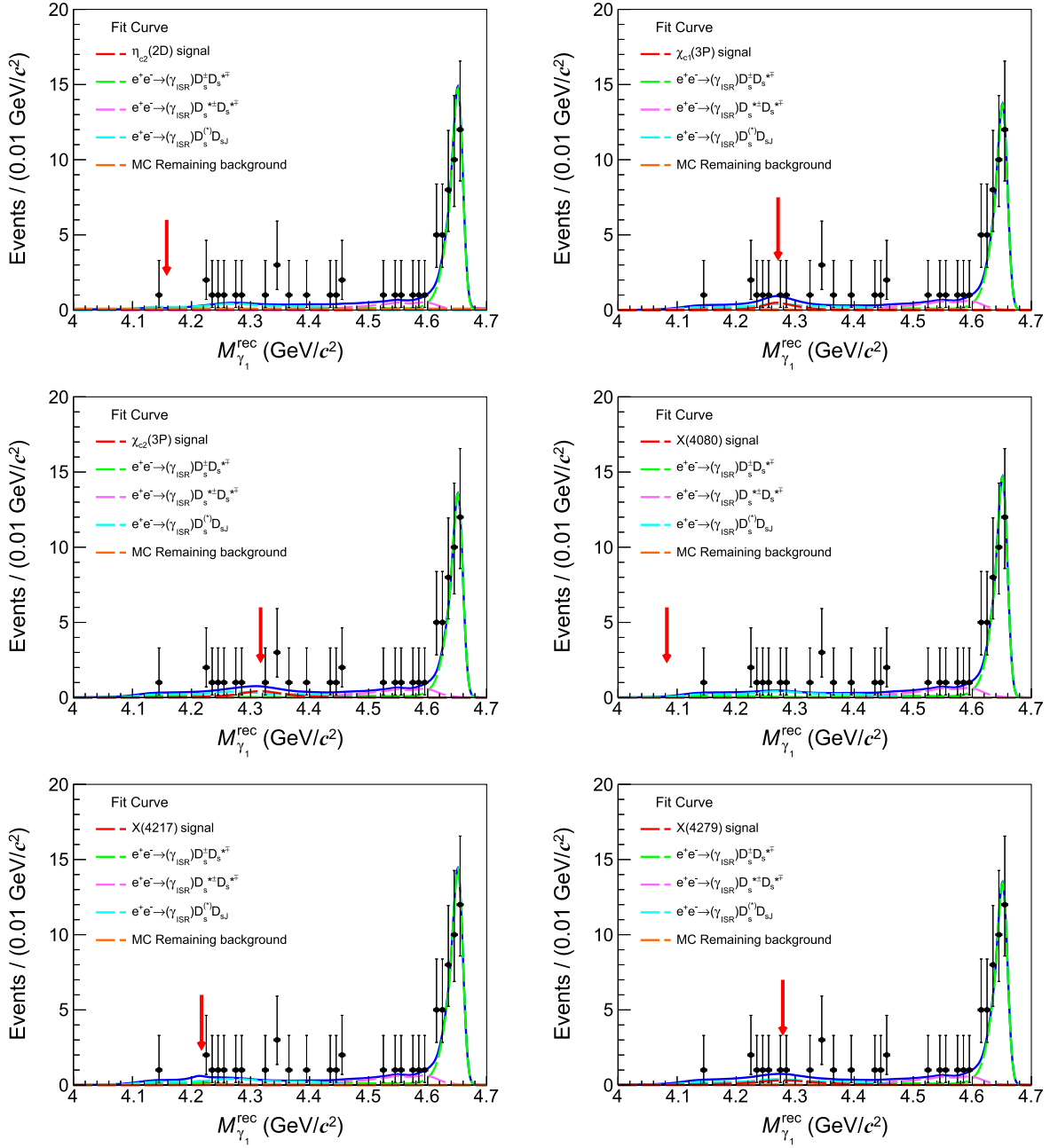
FIG. 1. Fits to the $M_{\gamma_1}^{rec}$ spectrum with masses and widths fixed to those of the $\eta_{c2}(2D)$, $\chi_{c1}(3P)$, $\chi_{c2}(3P)$, $X(4080)$, $X(4217)$, and $X(4279)$ as listed in Table I. The dots with error bars are the data distribution and the blue solid lines are the best fit results. The red arrows indicate the peak positions of those six X states with masses fixed to the predictions listed in Table I.

Gaussian function are obtained by using a control sample, $e^+e^- \to D_s^\pm D_s^{*\mp}$. The selection of the control sample is similar to that of the signal sample, except that only one photon is required instead of two. The D_s and D_s^* mass distributions from data are fitted with the line shape from MC samples convoluted with Gaussian functions. The parameters of the Gaussian function, representing the difference of the mass resolutions between data and MC simulation, are then used as the parameters of the Gaussian function in the extraction of the X signal yield.

The $B_{1(2)}$ line shape is taken from the $e^+e^- \to (\gamma_{ISR})D_s^\pm D_s^{*\mp}$ ($e^+e^- \to (\gamma_{ISR})D_s^{*\pm}D_s^{*\mp}$) MC simulation, B_3 is from the sum of the $e^+e^- \to (\gamma_{ISR})D_s^* D_{s0}^*(2317)$ and $(\gamma_{ISR})D_s^{(*)}D_{s1}(2460)$ MC simulations (weighted according to the product of the cross sections and detection efficiencies), and B_4 is modeled by a polynomial function.

Figure 1 shows the fit results where the masses and widths of the X states are fixed to the predictions listed in Table I. The signal yields are summarized in Table II. Since

TABLE II. Product of upper limits of Born cross section of $e^+e^- \to \gamma X$ and the branching fraction of $X \to D_s^{\pm} D_s^{*\mp}$ at 90% CL for each candidate *C*-even state, where f^r, f^v, N_{sig}, $N_{\text{sig}}^{\text{UL}}$, $N_{\text{bkg}1,2,4}$, and $\bar{\epsilon}$ are the ISR correction factor, the vacuum polarization correction factor, the number of signal events, the upper limit on the number of signal events, the numbers of background events, and the average detection efficiency, respectively. "$\sigma^{\text{UL}} \cdot \mathcal{B}$ with sys" stands for the upper limits of the cross section times the branching ratio with systematic uncertainties. "Significance" represents statistical significance.

	$\eta_{c2}(2D)$	$\chi_{c1}(3P)$	$\chi_{c2}(3P)$	$X(4080)$	$X(4217)$	$X(4279)$
f^r	1.06	1.06	1.06	1.06	1.06	1.06
f^v	1.05	1.05	1.05	1.05	1.05	1.05
$N_{\text{sig}}^{\text{UL}}$	5.2	10.1	11.4	2.4	6.0	12.2
N_{sig}	$-4.6^{+3.6}_{-2.9}$	$4.0^{+3.8}_{-3.0}$	$5.0^{+4.1}_{-3.3}$	$-0.3^{+0.3}_{-0.0}$	$1.1^{+2.7}_{-1.9}$	$5.3^{+4.5}_{-3.7}$
$N_{\text{bkg}1}$	$43.1^{+7.6}_{-7.0}$	$42.3^{+7.4}_{-6.7}$	$42.2^{+7.4}_{-6.7}$	$42.9^{+7.5}_{-6.8}$	$42.7^{+7.5}_{-6.8}$	$42.1^{+7.4}_{-6.7}$
$N_{\text{bkg}2}$	$6.6^{+4.8}_{-4.1}$	$8.2^{+4.3}_{-3.4}$	$7.9^{+4.2}_{-3.4}$	$8.2^{+4.3}_{-3.8}$	$8.3^{+4.3}_{-3.4}$	$7.8^{+4.2}_{-3.4}$
$N_{\text{bkg}4}$	$6.0^{+9.3}_{-0.0}$	$0.0^{+2.9}_{-0.0}$	$0.0^{+2.3}_{-0.0}$	$0.0^{+6.0}_{-0.0}$	$0.0^{+5.2}_{-0.0}$	$0.0^{+2.3}_{-0.0}$
Significance (σ)	$\cdots$	1.4	1.6	$\cdots$	0.5	1.5
$\bar{\epsilon}(10^{-4})$	3.73	3.48	3.26	4.21	3.50	3.11
$\sigma^{\text{UL}} \cdot \mathcal{B}$ with sys. (pb)	10.7	23.4	28.3	4.1	13.5	32.4

no events are retained near the $D_s^{\pm} D_s^{*\mp}$ mass threshold, the number of $X(4080)$ signal yields is calculated using $N_{\text{obs}} - N_{\text{bkg}(1,2,3,4)}$, where $N_{\text{obs}} = 0$ is the number of observed events, $N_{\text{bkg}(1,2,3,4)}$ are the numbers of background events obtained from the fit with N_{sig} set to zero. All the numbers are counted within [4.068, 4.098] GeV/c^2, which is about 3σ around the $X(4080)$ nominal mass. The statistical significance is evaluated by using $\sqrt{2\ln(L_{\text{max}}/L_0)]/(\Delta \text{ndf} = 1)}$, where $\ln L_{\text{max}}$ and $\ln L_0$ are the logarithmic likelihood values with and without the signal component in the fits, and Δndf is the change of the number of degrees of freedom. The upper limits of the number of signal events are calcualted using a Bayesian method [44] with a prior. The likelihood distribution, $L(x)$, is obtained by repeating the fit to the $M_{\gamma_1}^{\text{rec}}$ spectrum with a series of fixed values for the number of signal events, x. The upper limits at 90% confidence level (CL) are determined from $\int_0^{N_{\text{sig}}^{\text{UL}}} L(x)dx / \int_0^{\infty} L(x)dx = 0.9$, as listed in Table II.

In addition, upper limits for the signal cross sections as a function of the X masses in the range [4.08, 4.32] GeV/c^2 are also provided. From studies of simulation samples (Group-II), it is found the parameters $m_2 - m_1$, σ_2/σ_1, and f of the resolution function are very similar for various widths and J^{PC}. The parameters are found to be

$$m_2 - m_1 = (15.6 \pm 0.2) \text{ MeV}/c^2,$$
$$\sigma_2/\sigma_1 = 3.01 \pm 0.02,$$
$$f = 0.692 \pm 0.005, \quad (1)$$

using the MC sample with $\Gamma = 50$ MeV and $J^{PC} = 0^{-+}$, and they are fixed in the latter fit to $M_{\gamma_1}^{\text{rec}}$. The m_1 and σ_1 dependence on the mass of the X state are shown in Fig. 2.

A parametrization of the resolution, as a function of m_1 and σ_1 vs M_X distributions, is fitted with first order polynomial functions. The dependencies of m_1 and σ_1 on other width and J^{PC} are studied separately. The trends are similar to those shown in Fig. 2. The mass resolutions of the X in the region [4.08, 4.32] GeV/c^2 are evaluated from these fitted
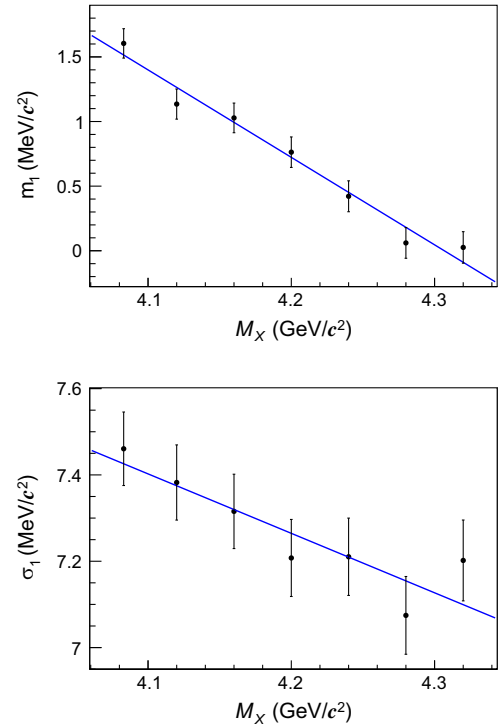

FIG. 2. M_X dependence of m_1 (upper) and σ_1 (lower) for $\Gamma = 50$ MeV and $J^{PC} = 0^{-+}$ according to MC simulation studies. The solid lines are the fit results.
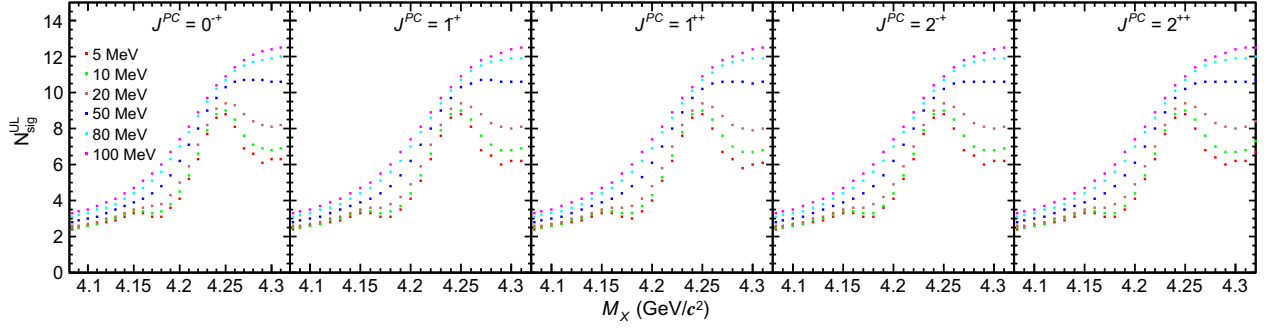
FIG. 3. Upper limits on the number of X signal events as a function of X mass for different quantum numbers ($J^{PC} = 0^{-+}$, 1^{-+}, 1^{++}, 2^{-+}, and 2^{++}) and widths of the X ($\Gamma = 5$ MeV, 10 MeV, 20 MeV, 50 MeV, 80 MeV, and 100 MeV).

function. The upper limits of the number of signal events as a function of the X mass for different X widths and quantum numbers are shown in Fig. 3.

V. CROSS SECTION CALCULATION

The Born cross section of $e^+e^- \to \gamma X$ times the branching fraction of $X \to D_s^\pm D_s^{*\mp}$ is calculated as

$$\sigma \cdot \mathcal{B}[X \to D_s^\pm D_s^{*\mp}] = \frac{N_{\text{sig}}}{\mathcal{L}_{\text{int}} f^r f^v \mathcal{B}[D_s^* \to \gamma D_s] \bar{\epsilon}}, \quad (2)$$

where N_{sig} is the number of signal events obtained from the fit; $\bar{\epsilon} = \sum_{j,k=1}^{2} \epsilon_{jk} \mathcal{B}_j \mathcal{B}_k$ represents the average detection efficiency, where ϵ_{jk} is the detection efficiency for $e^+e^- \to \gamma X, X \to D_s^\pm D_s^{*\mp}, D_s^{*\mp} \to \gamma D_s^\mp$, $D_s^+ \to j, D_s^- \to k$; and $\mathcal{B}_j$ ($\mathcal{B}_k$) is the branching fraction of $D_s^+ \to j$ ($D_s^- \to k$). Here j and k are the first and second decay modes of the D_s. The ISR correction factor ($f^r = (1 + \delta)$) is calculated following the procedure described in Refs. [31,32]. The vacuum polarization correction factor is $f^v = 1/|1 - \Pi|^2$ [45]. $\mathcal{B}[D_s^* \to \gamma D_s]$ is the branching fraction of $D_s^* \to \gamma D_s$. The results are summarized in Table II. The product of the upper limit of the cross section and the branching fraction ranges between 4 pb and 35 pb, depending on the mass and width of the X states.

Figure 4 illustrates the upper limits of $\sigma^{\text{UL}} \cdot \mathcal{B}[X \to D_s^\pm D_s^{*\mp}]$ under different assumptions of the mass, width, and J^{PC} of the X states after considering all the systematic uncertainties. Detailed descriptions of the systematic uncertainties are provided in the subsequent sections. The detection efficiency as a function of M for different width and J^{PC} assumptions of the X state is estimated from Group-II MC simulations. The M_X dependence of the detection efficiency is fitted with a first order polynomial function, as shown in Fig. 5.

In the calculation of the upper limits of Born cross sections displayed in Fig. 4, the detection efficiencies are extracted from the fitted curves and combined into the average detection efficiency $\bar{\epsilon}$.

VI. SYSTEMATIC UNCERTAINTY ESTIMATION

The systematic uncertainties on $\sigma \cdot \mathcal{B}$ are mainly originated from the luminosity measurement, the detection efficiency, the quoted branching fractions, the ISR correction factor, and the fit models. The uncertainty from the vacuum polarization correction is negligible. A summary of systematic uncertainties is given in Table III. The total systematic uncertainty is taken as a quadrature sum of each contribution:

(a) The integrated luminosity is measured using Bhabha scattering events, with an uncertainty of 1.0% [23].
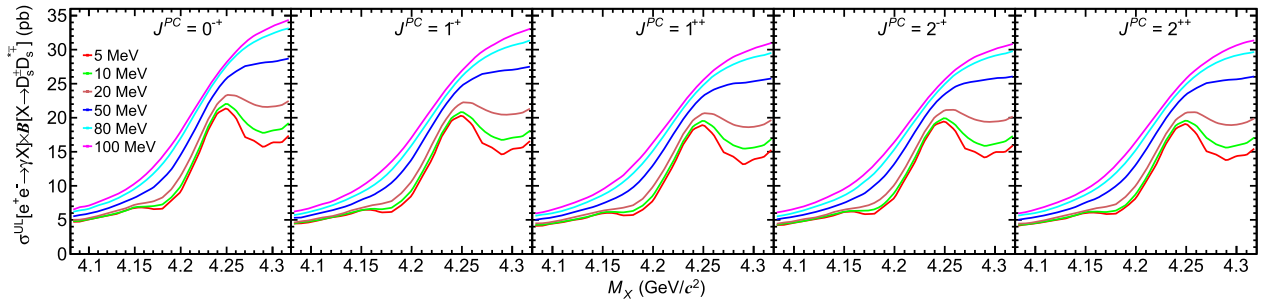

FIG. 4. Upper limits on $\sigma[e^+e^- \to \gamma X] \cdot \mathcal{B}[X \to D_s^\pm D_s^{*\mp}]$ as a function of X mass for different quantum numbers ($J^{PC} = 0^{-+}$, 1^{-+}, 1^{++}, 2^{-+}, and 2^{++}) and widths of the X ($\Gamma = 5$ MeV, 10 MeV, 20 MeV, 50 MeV, 80 MeV, and 100 MeV) after considering the systematic uncertainties.
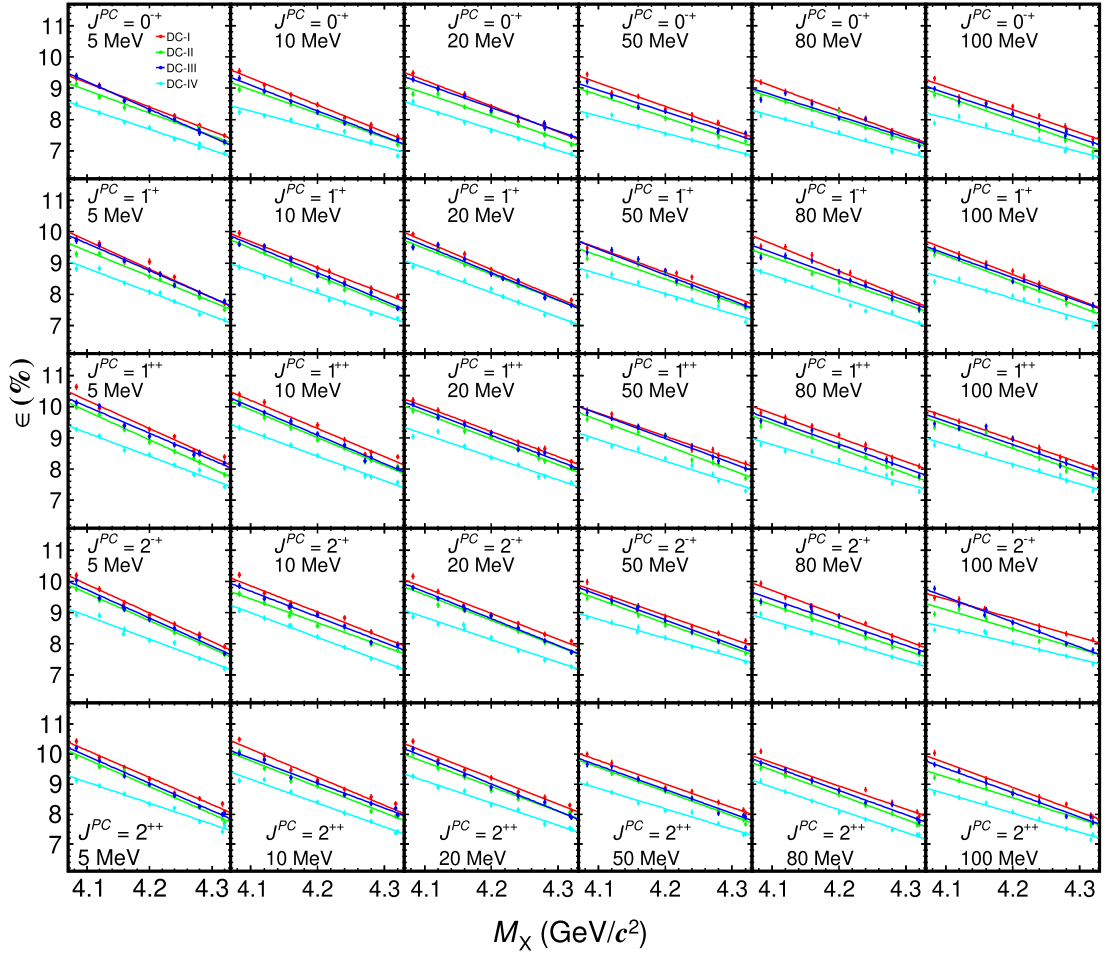
FIG. 5. M_X dependence of the efficiencies for the four channels for different J^{PC} and width assumptions. The lines are the fit results.

TABLE III.   Summary of systematic uncertainties (in %) for the Born cross section measurements.

Source	$J^{PC} = 0^{-+}$	1^{-+}	1^{++}	2^{-+}	2^{++}
Integrated luminosity	1.0	1.0	1.0	1.0	1.0
PID	5.7	5.7	5.7	5.7	5.7
Tracking	5.7	5.7	5.7	5.7	5.7
Photon reconstruction	2.0	2.0	2.0	2.0	2.0
K_S^0 reconstruction	0.4	0.4	0.4	0.4	0.4
Kinematic fit	0.7	0.7	0.8	0.8	0.7
D_s mass window	0.3	0.3	0.3	0.3	0.3
D_s^* mass window	0.1	0.1	0.1	0.1	0.1
ISR correction factor	24.6	24.4	23.8	23.5	23.7
Efficiency curve parameters	0.7	0.8	0.7	0.8	0.7
Efficiency curve parametrization	0.7	1.4	1.5	1.0	0.9
$\mathcal{B}(D_s^* \to \gamma D_s)$	0.8	0.8	0.8	0.8	0.8
$\mathcal{B}(D_s \to K^+ K^- \pi)$	3.3	3.3	3.3	3.3	3.3
$\mathcal{B}(D_s \to K_S^0 K)$	0.8	0.8	0.8	0.8	0.8
$\mathcal{B}(K_S^0 \to \pi^+ \pi^-)$	0.1	0.1	0.1	0.1	0.1
Total	26.3	26.1	25.5	25.2	25.4

(b) The difference in the tracking efficiencies between data and MC simulation is estimated to be 1.0% per track for that decay from IP [46–48]. There are six charged tracks in DC-I, four tracks in DC-II and DC-III, and two tracks in DC-IV. The charged tracks ($\pi^+\pi^-$) of the K_S^0 daughters are not counted. The detection efficiencies of the four channels are changed by $\pm m \cdot 1.0\%$ to recalculate the Born cross section, where m is the number of charged tracks in the channel. The larger difference to the nominal result, 5.7%, is taken as the systematic uncertainty.

(c) The systematic uncertainty from PID is 1.0% per π/K track [46–48]. This uncertainty is calculated using the same method as used for tracking efficiency, and 5.7% is taken as the systematic uncertainty.

(d) The systematic uncertainty of the photon reconstruction efficiency is 1.0% per photon [49] based on studies of the processes $\chi_{c0,2} \to \pi^0\pi^0, \eta\eta$. Because there are two photons in the final state, 2.0% is assigned as the systematic uncertainty.

(e) The K_S^0 reconstruction efficiency includes the geometric acceptance, tracking efficiency, and the candidate selection. The difference in the K_S^0 reconstruction efficiency between data and MC simulation is estimated with the control samples of $J/\psi \to K^*(892)^\pm K^\mp, K^*(892)^\pm \to K_S^0\pi^\pm$, and $J/\psi \to \phi K_S^0 K^\pm \pi^\mp$ [50] and is determined to be 1.2%. There is one K_S^0 candidate in DC-II and DC-III and two K_S^0 candidates in DC-IV. The detection efficiencies of the channels with K_S^0 in the final state are varied by $\pm n \cdot 1.2\%$, and the resulting detection efficiencies are used to calculate the Born cross section, where n is the number of K_S^0 in the channel. The systematic uncertainty for the K_S^0 reconstruction is estimated by the larger discrepancy between the two resulting Born cross sections and the nominal value.

(f) The systematic uncertainty caused by the 6C kinematic fit is estimated by correcting the helix parameters of the simulated charged tracks [51]. The result after correction is taken as the nominal one, and the difference between the results with and without this correction, 0.7% to 0.8%, is taken as the systematic uncertainty.

(g) The systematic uncertainties from the D_s and D_s^* mass window requirements are due to the mass resolution difference between data and MC. It is estimated by correcting the mass resolution in MC to improve the consistency between data and MC simulation. The correction is applied by smearing the MC distribution with a Gaussian function, and the parameters of the Gaussian function are obtained from the control sample of $e^+e^- \to D_s^\pm D_s^{*\mp}, D_s^{*\mp} \to \gamma D_s^\mp$. The mean and standard deviation of the Gaussian function are (0.3 ± 0.6) MeV/c^2 and (3.7 ± 0.9) MeV/c^2

for the D_s, (1.5 ± 1.1) MeV/c^2 and (0.5 ± 4.2) MeV/c^2 for the D_s^*. The selection efficiency difference with or without (used as nominal result) the smearing procedure is taken as the systematic uncertainty, which is 0.3% and 0.1% for the D_s and D_s^*, respectively.

(h) In the nominal results, the detection efficiency and the ISR correction factor are obtained by assuming the Born cross section of $e^+e^- \to \gamma X$ follows the line shape of the $\psi(4660)$, which is a well-established vector state in this energy region. Different shapes of the input cross sections result in different probabilities of generating events with the ISR photon. Assuming the branching fraction of $\psi(4660) \to \gamma X$ is small, the input cross section line shape is changed to E_γ^3/s (E_γ^3 term comes from the radiative transition rate [52] and $1/s$ is based on the assumption that the matrix element exhibits a similar c.m. energy dependence as the pure continuum process), where E_γ is energy of the radiative photon and s is the square of the center-of-mass energy. There is a large difference between the two input line shapes, which leads to large differences in the detection efficiencies and the ISR correction factors. The changes in the resultant Born cross sections are taken as the systematic uncertainty from the ISR correction factor [53].

(i) For the calculation of the Born cross section of $e^+e^- \to \gamma X, X \to D_s^\pm D_s^{*\mp}$ with different M under assumed Γ and J^{PC}, the detection efficiency is read from the fitted curves. The uncertainty in the efficiency induced by the fitted parameters is $\Delta\epsilon_{jk} = \sqrt{(m \cdot \Delta a_{jk})^2 + (\Delta b_{jk})^2 + 2 \cdot m \cdot \text{cov}(a_{jk}, b_{jk})}$, where a_{jk} and b_{jk} are the parameters of the polynomial function, Δa_{jk} and Δb_{jk} are the corresponding uncertainties, and $\text{cov}(a_{jk}, b_{jk})$ is the covariance between a_{jk} and b_{jk} given by the corresponding fit. The detection efficiency, ϵ_{jk}, is varied by $\pm\Delta\epsilon_{jk}$, and the difference on the efficiency is taken as the systematic uncertainty.

(j) The systematic uncertainty from the parametrization of the efficiency curves is estimated by changing the fitted function from a first-order to a second-order polynomial function. The average detection efficiency is recalculated with parameters from the alternative fitted curves. The largest difference between the nominal and each fit result is taken as the systematic uncertainty.

(k) The branching fractions of $D_s \to K^+K^-\pi$, $D_s \to K_S^0 K$, $D_s^* \to \gamma D_s$, and $K_S^0 \to \pi^+\pi^-$ are taken from the PDG [35], and their uncertainties are propagated to the Born cross section measurement. The systematic uncertainties caused by the branching fractions of $D_s \to K^+K^-\pi$, $D_s \to K_S^0 K$, $D_s^* \to \gamma D_s$,

and $K_S^0 \to \pi^+\pi^-$ are 3.3%, 0.8%, 0.8%, and 0.1%, respectively.

(l) The fit-related systematic uncertainties are estimated by varying the fit models. The largest upper limit on the number of signal events is taken as the upper limit of the Born cross section with the systematic uncertainty considered. The line shapes of the background contributions from $e^+e^- \to (\gamma_{\mathrm{ISR}})D_s^{\pm(*)}D_s^{*\mp}$ are taken from the MC simulations with the latest precise measurements as input. The uncertainties are found to be negligible. The systematic uncertainty from the fixed number of background events for the processes $e^+e^- \to (\gamma_{\mathrm{ISR}})D_s^{(*)}D_{sJ}$ is estimated by modifying N_{bkg3} with $\pm 1 \cdot \sigma$. The uncertainty arising from the modeling of the remaining background events is accessed by replacing the zero-order polynomial function with the line shape extracted from generic MC simulation. In the determination of the upper limit of the number of signal events with different M under assumed width and J^{PC}, the mass resolutions are read from the fit curves shown in Fig. 2. The systematic uncertainties from $m_1 - m_2, \sigma_2/\sigma_1$, and f are considered by varying the parameters within their uncertainties, while the systematic uncertainties from m_1 and σ_1, are considered by varying Δm_1 and $\Delta \sigma_1$. The largest upper limit on the number of signal events is taken, where Δm_1 and $\Delta \sigma_1$ are calculated using the same formula as used to calculate $\Delta \epsilon_{jk}$. To take into account the systematic uncertainties in the upper limit calculation, the likelihood distributions are convolved with Gaussian functions as

$$L'(x) = \int_0^1 L(x; N_{\mathrm{sig}}\bar{\epsilon}/\hat{\epsilon}) \exp\left[-\frac{(\bar{\epsilon} - \hat{\epsilon})^2}{2\sigma_{\mathrm{sys.}}^2}\right] d\bar{\epsilon},$$

where $\hat{\epsilon}$ is the nominal average detection efficiency, and σ_{sys} is the systematic uncertainty [44,54]. The upper limit of the Born cross section times the branching fraction with fixed masses and widths are listed in Table II. The upper limits of $\sigma[e^+e^- \to \gamma X] \cdot \mathcal{B}[X \to D_s^{\pm}D_s^{*\mp}]$ as a function of X mass after considering all the systematic uncertainties are displayed in Fig. 4.

VII. SUMMARY

In summary, based on a data sample collected at $\sqrt{s} = (4681.92 \pm 0.08 \pm 0.29)$ MeV with an integrated luminosity of $(1667.39 \pm 0.21 \pm 8.84)$ pb^{-1}, a search for C-even states is performed via the process $e^+e^- \to \gamma D_s^{\pm}D_s^{*\mp}$. No statistically significant signals are observed. Upper limits on $\sigma[e^+e^- \to \gamma X] \cdot \mathcal{B}[X \to D_s^{\pm}D_s^{*\mp}]$ $[X = \eta_{c2}(2D), \chi_{c1}(3P), \chi_{c2}(3P), X(4080), X(4217)$, and $X(4279)]$ at 90% CL are

determined to be 10.7 pb, 23.4 pb, 28.3 pb, 4.1 pb, 13.5 pb, and 32.4 pb, respectively. Upper limits with other mass and width assumptions are also calculated and shown in Fig. 4. Furthermore, the product of the upper limit of the cross section and the branching fraction is between 4 pb to 35 pb. Due to statistical limitations, the upper limit for $\psi(4660) \to \gamma\chi_{c1,2}(3P)$ is below the sensitivity of the theoretical prediction in Ref. [55]. There is no other theoretical prediction for the cross sections of other C-even states. More data samples and theoretical calculations are needed to investigate the EM transition properties of $\psi(4660)$.

[1] S. Okubo, Phys. Lett. **5**, 165 (1963).
[2] G. Zweig, CERN Preprints TH 401 and TH 412.
[3] J. Iizuka, Prog. Theor. Phys. Suppl. **37**, 21 (1966).
[4] T. Barnes, S. Godfrey, and E. S. Swanson, Phys. Rev. D **72**, 054026 (2005).
[5] S. Godfrey and N. Isgur, Phys. Rev. D **32**, 189 (1985).
[6] R. Aaij *et al.* (LHCb Collaboration), Phys. Rev. Lett. **127**, 082001 (2021).
[7] R. Aaij *et al.* (LHCb Collaboration), Phys. Rev. Lett. **118**, 022003 (2017).
[8] R. Aaij *et al.* (LHCb Collaboration), Phys. Rev. D **95**, 012002 (2017).
[9] X. K. Dong, F. K. Guo, and B. S. Zou, Progr. Phys. **41**, 65 (2021).
[10] L. Liu, G. Moir, M. Peardon, S. M. Ryan, C. E. Thomas, P. Vilaseca, J. J. Dudek, R. G. Edwards, B. Joó, and D. G. Richards (Hadron Spectrum Collaboration), J. High Energy Phys. 07 (2012) 126.
[11] G. K. Cheung, C. O'Hara, G. Moir, M. Peardon, S. M. Ryan, C. E. Thomas, and D. Tims (Hadron Spectrum Collaboration), J. High Energy Phys. 12 (2016) 089.
[12] C. Farina, H. Garcia Tecocoatzi, A. Giachino, E. Santopinto, and E. S. Swanson, Phys. Rev. D **102**, 014023 (2020).
[13] S. Choi *et al.* (Belle Collaboration), Phys. Rev. Lett. **91**, 262001 (2003).
[14] M. Ablikim *et al.* (BESIII Collaboration), Phys. Rev. Lett. **110**, 252001 (2013).
[15] Z. Liu *et al.* (Belle Collaboration), Phys. Rev. Lett. **110**, 252002 (2013); **111**, 019901(E) (2013).
[16] M. Ablikim *et al.* (BESIII Collaboration), Phys. Rev. Lett. **112**, 022001 (2014).
[17] M. Ablikim *et al.* (BESIII Collaboration), Phys. Rev. Lett. **111**, 242001 (2013).
[18] M. Ablikim *et al.* (BESIII Collaboration), Phys. Rev. Lett. **112**, 132001 (2014).
[19] M. Ablikim *et al.* (BESIII Collaboration), Phys. Rev. Lett. **126**, 102001 (2021).
[20] M. Ablikim *et al.* (BESIII Collaboration), Phys. Rev. Lett. **129**, 112003 (2022).
[21] M. Ablikim *et al.* (BESIII Collaboration), Phys. Rev. Lett. **112**, 092001 (2014).
[22] M. Ablikim *et al.* (BESIII Collaboration), Phys. Rev. D **104**, 092001 (2021).
[23] M. Ablikim *et al.* (BESIII Collaboration), Chin. Phys. C **46**, 113003 (2022).
[24] M. Ablikim *et al.* (BESIII Collaboration), Nucl. Instrum. Methods Phys. Res., Sect. A **614**, 345 (2010).
[25] C. H. Yu *et al.*, *Proceedings of IPAC 2016, Busan, Korea* (2016), http://accelconf.web.cern.ch/ipac2016/doi/JACoW-IPAC2016-TUYA01.html.
[26] M. Ablikim *et al.* (BESIII Collaboration), Chin. Phys. C **44**, 040001 (2020).
[27] X. Li *et al.*, Radiat. Detect. Technol. Methods **1**, 13 (2017).
[28] Y. X. Guo *et al.*, Radiat. Detect. Technol. Methods **1**, 15 (2017).
[29] P. Cao *et al.*, Nucl. Instrum. Methods Phys. Res., Sect. A **953**, 163053 (2020).
[30] S. Agostinelli *et al.* (GEANT4 Collaboration), Nucl. Instrum. Methods Phys. Res., Sect. A **506**, 250 (2003).
[31] S. Jadach, B. F. L. Ward, and Z. Was, Comput. Phys. Commun. **130**, 260 (2000).
[32] S. Jadach, B. F. L. Ward, and Z. Was, Phys. Rev. D **63**, 113009 (2001).
[33] D. J. Lange, Nucl. Instrum. Methods Phys. Res., Sect. A **462**, 152 (2001).
[34] R. G. Ping, Chin. Phys. C **32**, 599 (2008).
[35] R. L. Workman *et al.* (Particle Data Group), Prog. Theor. Exp. Phys. **2022**, 083C01 (2022).
[36] J. C. Chen, G. S. Huang, X. R. Qi, D. H. Zhang, and Y. S. Zhu, Phys. Rev. D **62**, 034003 (2000).
[37] R. L. Yang, R. G. Ping, and H. Chen, Chin. Phys. Lett. **31**, 061301 (2014).
[38] P. Golonka and Z. Was, Eur. Phys. J. C **45**, 97 (2006).
[39] P. U. E. Onyisi *et al.* (CLEO Collaboration), Phys. Rev. D **88**, 032009 (2013).
[40] M. Ablikim *et al.* (BESIII Collaboration), Phys. Rev. D **104**, 012016 (2021).
[41] M. Ablikim *et al.* (BESIII Collaboration), Phys. Rev. Lett. **131**, 151903 (2023).
[42] M. Ablikim *et al.* (BESIII Collaboration), Phys. Rev. D **101**, 112008 (2020).
[43] M. Ablikim *et al.* (BESIII Collaboration), Phys. Rev. D **104**, 032012 (2021).
[44] J. Conrad, O. Botner, A. Hallgren, and C. Pérez de los Heros, Phys. Rev. D **67**, 012002 (2003).
[45] F. Jegerlehner, Nuovo Cimento C **034S1**, 31 (2011).
[46] W. L. Yuan, X. C. Ai, X. B. Ji, S. J. Chen, Y. Zhang, L. H. Wu, L. L. Wang, and Y. Yuan, Chin. Phys. C **40**, 026201 (2016).
[47] M. Ablikim *et al.* (BESIII Collaboration), Phys. Rev. D **86**, 092009 (2012).
[48] M. Ablikim *et al.* (BESIII Collaboration), Phys. Rev. D **83**, 112005 (2011).
[49] M. Ablikim *et al.* (BESIII Collaboration), Phys. Rev. D **81**, 052005 (2010).
[50] M. Ablikim *et al.* (BESIII Collaboration), Phys. Rev. D **92**, 112008 (2015).
[51] M. Ablikim *et al.* (BESIII Collaboration), Phys. Rev. D **87**, 012002 (2013).
[52] N. Brambilla *et al.* (Quarkonium Working Group), arXiv:hep-ph/0412158.
[53] W. Y. Sun, T. Liu, M. Q. Jing, L. L. Wang, B. Zhong, and W. M. Song, Front. Phys. **16**, 64501 (2021).
[54] Olaf Behnke, Kevin Kröninger, Grégory Schott, and Thomas Schörner-Sadenius, *Data Analysis in High Energy Physics: A Practical Guide to Statistical Methods* (Wiley-VCH, New York, 2013).
[55] G. J. Ding, J. J. Zhu, and M. L. Yan, Phys. Rev. D **77**, 014033 (2008).

M. Ablikim,[1] M. N. Achasov,[4,c] P. Adlarson,[75] O. Afedulidis,[3] X. C. Ai,[80] R. Aliberti,[35] A. Amoroso,[74a,74c] Q. An,[71,58,a] Y. Bai,[57] O. Bakina,[36] I. Balossino,[29a] Y. Ban,[46,h] H.-R. Bao,[63] V. Batozskaya,[1,44] K. Begzsuren,[32] N. Berger,[35] M. Berlowski,[44] M. Bertani,[28a] D. Bettoni,[29a] F. Bianchi,[74a,74c] E. Bianco,[74a,74c] A. Bortone,[74a,74c] I. Boyko,[36] R. A. Briere,[5] A. Brueggemann,[68] H. Cai,[76] X. Cai,[1,58] A. Calcaterra,[28a] G. F. Cao,[1,63] N. Cao,[1,63] S. A. Cetin,[62a] J. F. Chang,[1,58] G. R. Che,[43] G. Chelkov,[36,b] C. Chen,[43] C. H. Chen,[9] Chao Chen,[55] G. Chen,[1] H. S. Chen,[1,63] H. Y. Chen,[20] M. L. Chen,[1,58,63] S. J. Chen,[42] S. L. Chen,[45] S. M. Chen,[61] T. Chen,[1,63] X. R. Chen,[31,63] X. T. Chen,[1,63] Y. B. Chen,[1,58] Y. Q. Chen,[34] Z. J. Chen,[25,i] Z. Y. Chen,[1,63] S. K. Choi,[10] G. Cibinetto,[29a] F. Cossio,[74c] J. J. Cui,[50] H. L. Dai,[1,58] J. P. Dai,[78] A. Dbeyssi,[18] R. E. de Boer,[3] D. Dedovich,[36] C. Q. Deng,[72] Z. Y. Deng,[1] A. Denig,[35] I. Denysenko,[36] M. Destefanis,[74a,74c] F. De Mori,[74a,74c] B. Ding,[66,1] X. X. Ding,[46,h] Y. Ding,[34] Y. Ding,[40] J. Dong,[1,58] L. Y. Dong,[1,63] M. Y. Dong,[1,58,63] X. Dong,[76] M. C. Du,[1] S. X. Du,[80] Y. Y. Duan,[55] Z. H. Duan,[42] P. Egorov,[36,b] Y. H. Fan,[45] J. Fang,[59] J. Fang,[1,58] S. S. Fang,[1,63] W. X. Fang,[1] Y. Fang,[1] Y. Q. Fang,[1,58] R. Farinelli,[29a] L. Fava,[74b,74c] F. Feldbauer,[3] G. Felici,[28a] C. Q. Feng,[71,58] J. H. Feng,[59] Y. T. Feng,[71,58] M. Fritsch,[3] C. D. Fu,[1] J. L. Fu,[63] Y. W. Fu,[1,63] H. Gao,[63] X. B. Gao,[41] Y. N. Gao,[46,h] Yang Gao,[71,58] S. Garbolino,[74c] I. Garzia,[29a,29b] L. Ge,[80] P. T. Ge,[76] Z. W. Ge,[42] C. Geng,[59] E. M. Gersabeck,[67] A. Gilman,[69] K. Goetzen,[13] L. Gong,[40] W. X. Gong,[1,58] W. Gradl,[35] S. Gramigna,[29a,29b] M. Greco,[74a,74c] M. H. Gu,[1,58] Y. T. Gu,[15] C. Y. Guan,[1,63] Z. L. Guan,[22] A. Q. Guo,[31,63] L. B. Guo,[41] M. J. Guo,[50] R. P. Guo,[49] Y. P. Guo,[12,g] A. Guskov,[36,b] J. Gutierrez,[27] K. L. Han,[63] T. T. Han,[1] F. Hanisch,[3] X. Q. Hao,[19] F. A. Harris,[65] K. K. He,[55] K. L. He,[1,63] F. H. Heinsius,[3] C. H. Heinz,[35] Y. K. Heng,[1,58,63] C. Herold,[60] T. Holtmann,[3] P. C. Hong,[34] G. Y. Hou,[1,63] X. T. Hou,[1,63] Y. R. Hou,[63] Z. L. Hou,[1] B. Y. Hu,[59] H. M. Hu,[1,63] J. F. Hu,[56,j] S. L. Hu,[12,g] T. Hu,[1,58,63] Y. Hu,[1] G. S. Huang,[71,58] K. X. Huang,[59] L. Q. Huang,[31,63] X. T. Huang,[50] Y. P. Huang,[1] T. Hussain,[73] F. Hölzken,[3] N. Hüsken,[27,35] N. Hüsken,[35] N. in der Wiesche,[68] J. Jackson,[27] S. Janchiv,[32] J. H. Jeong,[10] Q. Ji,[1] Q. P. Ji,[19] W. Ji,[1,63] X. B. Ji,[1,63] X. L. Ji,[1,58] Y. Y. Ji,[50] X. Q. Jia,[50] Z. K. Jia,[71,58] D. Jiang,[1,63] H. B. Jiang,[76] P. C. Jiang,[46,h] S. S. Jiang,[39] T. J. Jiang,[16] X. S. Jiang,[1,58,63] Y. Jiang,[63] J. B. Jiao,[50] J. K. Jiao,[34] Z. Jiao,[23] S. Jin,[42] Y. Jin,[66] M. Q. Jing,[1,63] X. M. Jing,[63] T. Johansson,[75] S. Kabana,[33] N. Kalantar-Nayestanaki,[64] X. L. Kang,[9] X. S. Kang,[40] M. Kavatsyuk,[64] B. C. Ke,[80] V. Khachatryan,[27] A. Khoukaz,[68] R. Kiuchi,[1] O. B. Kolcu,[62a] B. Kopf,[3] M. Kuessner,[3] X. Kui,[1,63] N. Kumar,[26] A. Kupsc,[44,75] W. Kühn,[37] J. J. Lane,[67] P. Larin,[18] L. Lavezzi,[74a,74c] T. T. Lei,[71,58] Z. H. Lei,[71,58] M. Lellmann,[35] T. Lenz,[35] C. Li,[47] C. Li,[43] C. H. Li,[39] Cheng Li,[71,58] D. M. Li,[80] F. Li,[1,58] G. Li,[1] H. B. Li,[1,63] H. J. Li,[19] H. N. Li,[56,j] Hui Li,[43] J. R. Li,[61] J. S. Li,[59] Ke Li,[1] L. J. Li,[1,63] L. K. Li,[1] Lei Li,[48] M. H. Li,[43] P. R. Li,[38,l] Q. M. Li,[1,63] Q. X. Li,[50] R. Li,[17,31] S. X. Li,[12] T. Li,[50] W. D. Li,[1,63] W. G. Li,[1,a] X. Li,[1,63] X. H. Li,[71,58] X. L. Li,[50] X. Z. Li,[59] Xiaoyu Li,[1,63] Y. G. Li,[46,h] Z. J. Li,[59] Z. X. Li,[15] Z. Y. Li,[78] C. Liang,[42] H. Liang,[71,58] H. Liang,[1,63] Y. F. Liang,[54] Y. T. Liang,[31,63] G. R. Liao,[14] L. Z. Liao,[50] J. Libby,[26] A. Limphirat,[60] C. C. Lin,[55] D. X. Lin,[31,63] T. Lin,[1] B. J. Liu,[1] B. X. Liu,[76] C. Liu,[34] C. X. Liu,[1] F. H. Liu,[53] Fang Liu,[1] Feng Liu,[6] G. M. Liu,[56,j] H. Liu,[38,k,l] H. B. Liu,[15] H. M. Liu,[1,63] Huanhuan Liu,[1] Huihui Liu,[21] J. B. Liu,[71,58] J. Y. Liu,[1,63] K. Liu,[38,k,l] K. Y. Liu,[40] Ke Liu,[22] L. Liu,[71,58] L. C. Liu,[43] Lu Liu,[43] M. H. Liu,[12,g] P. L. Liu,[1] Q. Liu,[63] S. B. Liu,[71,58] T. Liu,[12,g] W. K. Liu,[43] W. M. Liu,[71,58] X. Liu,[39] X. Liu,[38,k,l] Y. Liu,[38,k,l] Y. Liu,[80] Y. B. Liu,[43] Z. A. Liu,[1,58,63] Z. D. Liu,[9] Z. Q. Liu,[50] X. C. Lou,[1,58,63] F. X. Lu,[59] H. J. Lu,[23] J. G. Lu,[1,58] X. L. Lu,[1] Y. Lu,[7] Y. P. Lu,[1,58] Z. H. Lu,[1,63] C. L. Luo,[41] M. X. Luo,[79] T. Luo,[12,g] X. L. Luo,[1,58] X. R. Lyu,[63] Y. F. Lyu,[43] F. C. Ma,[40] H. Ma,[78] H. L. Ma,[1] J. L. Ma,[1,63] L. L. Ma,[50] M. M. Ma,[1,63] Q. M. Ma,[1] R. Q. Ma,[1,63] T. Ma,[71,58] X. T. Ma,[1,63] X. Y. Ma,[1,58] Y. Ma,[46,h] Y. M. Ma,[31] F. E. Maas,[18] M. Maggiora,[74a,74c] S. Malde,[69] Y. J. Mao,[46,h] Z. P. Mao,[1] S. Marcello,[74a,74c] Z. X. Meng,[66] J. G. Messchendorp,[13,64] G. Mezzadri,[29a] H. Miao,[1,63] T. J. Min,[42] R. E. Mitchell,[27] X. H. Mo,[1,58,63] B. Moses,[27] N. Yu. Muchnoi,[4,c] J. Muskalla,[35] Y. Nefedov,[36] F. Nerling,[18,e] L. S. Nie,[20] I. B. Nikolaev,[4,c] Z. Ning,[1,58] S. Nisar,[11,m] Q. L. Niu,[38,k,l] W. D. Niu,[55] Y. Niu,[50] S. L. Olsen,[63] Q. Ouyang,[1,58,63] S. Pacetti,[28b,28c] X. Pan,[55] Y. Pan,[57] A. Pathak,[34] P. Patteri,[28a] Y. P. Pei,[71,58] M. Pelizaeus,[3] H. P. Peng,[71,58] Y. Y. Peng,[38,k,l] K. Peters,[13,e] J. L. Ping,[41] R. G. Ping,[1,63] S. Plura,[35] V. Prasad,[33] F. Z. Qi,[1] H. Qi,[71,58] H. R. Qi,[61] M. Qi,[42] T. Y. Qi,[12,g] S. Qian,[1,58] W. B. Qian,[63] C. F. Qiao,[63] X. K. Qiao,[80] J. J. Qin,[72] L. Q. Qin,[14] L. Y. Qin,[71,58] X. S. Qin,[50] Z. H. Qin,[1,58] J. F. Qiu,[1] Z. H. Qu,[72] C. F. Redmer,[35] K. J. Ren,[39] A. Rivetti,[74c] M. Rolo,[74c] G. Rong,[1,63] Ch. Rosner,[18] S. N. Ruan,[43] N. Salone,[44] A. Sarantsev,[36,d] Y. Schelhaas,[35] K. Schoenning,[75] M. Scodeggio,[29a] K. Y. Shan,[12,g] W. Shan,[24] X. Y. Shan,[71,58] Z. J. Shang,[38,k,l] J. F. Shangguan,[55] L. G. Shao,[1,63] M. Shao,[71,58] C. P. Shen,[12,g] H. F. Shen,[1,8] W. H. Shen,[63] X. Y. Shen,[1,63] B. A. Shi,[63] H. Shi,[71,58] H. C. Shi,[71,58] J. L. Shi,[12,g] J. Y. Shi,[1] Q. Q. Shi,[55] S. Y. Shi,[72] X. Shi,[1,58] J. J. Song,[19] T. Z. Song,[59] W. M. Song,[34,1] Y. J. Song,[12,g] Y. X. Song,[46,h,n] S. Sosio,[74a,74c] S. Spataro,[74a,74c] F. Stieler,[35] Y. J. Su,[63] G. B. Sun,[76] G. X. Sun,[1] H. Sun,[63] H. K. Sun,[1] J. F. Sun,[19] K. Sun,[61] L. Sun,[76] S. S. Sun,[1,63] T. Sun,[51,f] W. Y. Sun,[34] Y. Sun,[9] Y. J. Sun,[71,58] Y. Z. Sun,[1] Z. Q. Sun,[1,63] Z. T. Sun,[50] C. J. Tang,[54] G. Y. Tang,[1] J. Tang,[59] M. Tang,[71,58] Y. A. Tang,[76] L. Y. Tao,[72]

Q. T. Tao,[25,i] M. Tat,[69] J. X. Teng,[71,58] V. Thoren,[75] W. H. Tian,[59] Y. Tian,[31,63] Z. F. Tian,[76] I. Uman,[62b] Y. Wan,[55] S. J. Wang,[50] B. Wang,[1] B. L. Wang,[63] Bo Wang,[71,58] D. Y. Wang,[46,h] F. Wang,[72] H. J. Wang,[38,k,l] J. J. Wang,[76] J. P. Wang,[50] K. Wang,[1,58] L. L. Wang,[1] M. Wang,[50] Meng Wang,[1,63] N. Y. Wang,[63] S. Wang,[38,k,l] S. Wang,[12,g] T. Wang,[12,g] T. J. Wang,[43] W. Wang,[72] W. Wang,[59] W. P. Wang,[35,71,o] X. Wang,[46,h] X. F. Wang,[38,k,l] X. J. Wang,[39] X. L. Wang,[12,g] X. N. Wang,[1] Y. Wang,[61] Y. D. Wang,[45] Y. F. Wang,[1,58,63] Y. L. Wang,[19] Y. N. Wang,[45] Y. Q. Wang,[1] Yaqian Wang,[17] Yi Wang,[61] Z. Wang,[1,58] Z. L. Wang,[72] Z. Y. Wang,[1,63] Ziyi Wang,[63] D. H. Wei,[14] F. Weidner,[68] S. P. Wen,[1] Y. R. Wen,[39] U. Wiedner,[3] G. Wilkinson,[69] M. Wolke,[75] L. Wollenberg,[3] C. Wu,[39] J. F. Wu,[1,8] L. H. Wu,[1] L. J. Wu,[1,63] X. Wu,[12,g] X. H. Wu,[34] Y. Wu,[71,58] Y. H. Wu,[55] Y. J. Wu,[31] Z. Wu,[1,58] L. Xia,[71,58] X. M. Xian,[39] B. H. Xiang,[1,63] T. Xiang,[46,h] D. Xiao,[38,k,l] G. Y. Xiao,[42] S. Y. Xiao,[1] Y. L. Xiao,[12,g] Z. J. Xiao,[41] C. Xie,[42] X. H. Xie,[46,h] Y. Xie,[50] Y. G. Xie,[1,58] Y. H. Xie,[6] Z. P. Xie,[71,58] T. Y. Xing,[1,63] C. F. Xu,[1,63] C. J. Xu,[59] G. F. Xu,[1] H. Y. Xu,[66] M. Xu,[71,58] Q. J. Xu,[16] Q. N. Xu,[30] W. Xu,[1] W. L. Xu,[66] X. P. Xu,[55] Y. C. Xu,[77] Z. P. Xu,[42] Z. S. Xu,[63] F. Yan,[12,g] L. Yan,[12,g] W. B. Yan,[71,58] W. C. Yan,[80] X. Q. Yan,[1] H. J. Yang,[51,f] H. L. Yang,[34] H. X. Yang,[1] Tao Yang,[1] Y. Yang,[12,g] Y. F. Yang,[43] Y. X. Yang,[1,63] Yifan Yang,[1,63] Z. W. Yang,[38,k,l] Z. P. Yao,[50] M. Ye,[1,58] M. H. Ye,[8] J. H. Yin,[1] Z. Y. You,[59] B. X. Yu,[1,58,63] C. X. Yu,[43] G. Yu,[1,63] J. S. Yu,[25,i] T. Yu,[72] X. D. Yu,[46,h] Y. C. Yu,[80] C. Z. Yuan,[1,63] J. Yuan,[34] L. Yuan,[2] S. C. Yuan,[1] Y. Yuan,[1,63] Y. J. Yuan,[45] Z. Y. Yuan,[59] C. X. Yue,[39] A. A. Zafar,[73] F. R. Zeng,[50] S. H. Zeng,[72] X. Zeng,[12,g] Y. Zeng,[25,i] Y. J. Zeng,[59] X. Y. Zhai,[34] Y. C. Zhai,[50] Y. H. Zhan,[59] A. Q. Zhang,[1,63] B. L. Zhang,[1,63] B. X. Zhang,[1] D. H. Zhang,[43] G. Y. Zhang,[19] H. Zhang,[80] H. Zhang,[71,58] H. C. Zhang,[1,58,63] H. H. Zhang,[59] H. H. Zhang,[34] H. Q. Zhang,[1,58,63] H. R. Zhang,[71,58] H. Y. Zhang,[1,58] J. Zhang,[80] J. Zhang,[59] J. J. Zhang,[52] J. L. Zhang,[20] J. Q. Zhang,[41] J. S. Zhang,[12,g] J. W. Zhang,[1,58,63] J. X. Zhang,[38,k,l] J. Y. Zhang,[1] J. Z. Zhang,[1,63] Jianyu Zhang,[63] L. M. Zhang,[61] Lei Zhang,[42] P. Zhang,[1,63] Q. Y. Zhang,[34] R. Y. Zhang,[38,k,l] Shuihan Zhang,[1,63] Shulei Zhang,[25,i] X. D. Zhang,[45] X. M. Zhang,[1] X. Y. Zhang,[50] Y. Zhang,[72] Y. T. Zhang,[80] Y. H. Zhang,[1,58] Y. M. Zhang,[39] Yan Zhang,[71,58] Yao Zhang,[1] Z. D. Zhang,[1] Z. H. Zhang,[1] Z. L. Zhang,[34] Z. Y. Zhang,[76] Z. Y. Zhang,[43] Z. Z. Zhang,[45] G. Zhao,[1] J. Y. Zhao,[1,63] J. Z. Zhao,[1,58] Lei Zhao,[71,58] Ling Zhao,[1] M. G. Zhao,[43] N. Zhao,[78] R. P. Zhao,[63] S. J. Zhao,[80] Y. B. Zhao,[1,58] Y. X. Zhao,[31,63] Z. G. Zhao,[71,58] A. Zhemchugov,[36,b] B. Zheng,[72] B. M. Zheng,[34] J. P. Zheng,[1,58] W. J. Zheng,[1,63] Y. H. Zheng,[63] B. Zhong,[41] X. Zhong,[59] H. Zhou,[50] J. Y. Zhou,[34] L. P. Zhou,[1,63] S. Zhou,[6] X. Zhou,[76] X. K. Zhou,[6] X. R. Zhou,[71,58] X. Y. Zhou,[39] Y. Z. Zhou,[12,g] J. Zhu,[43] K. Zhu,[1] K. J. Zhu,[1,58,63] K. S. Zhu,[12,g] L. Zhu,[34] L. X. Zhu,[63] S. H. Zhu,[70] S. Q. Zhu,[42] T. J. Zhu,[12,g] W. D. Zhu,[41] Y. C. Zhu,[71,58] Z. A. Zhu,[1,63] J. H. Zou,[1] and J. Zu[71,58]

(BESIII Collaboration)

[1]*Institute of High Energy Physics, Beijing 100049, People's Republic of China*
[2]*Beihang University, Beijing 100191, People's Republic of China*
[3]*Bochum Ruhr-University, D-44780 Bochum, Germany*
[4]*Budker Institute of Nuclear Physics SB RAS (BINP), Novosibirsk 630090, Russia*
[5]*Carnegie Mellon University, Pittsburgh, Pennsylvania 15213, USA*
[6]*Central China Normal University, Wuhan 430079, People's Republic of China*
[7]*Central South University, Changsha 410083, People's Republic of China*
[8]*China Center of Advanced Science and Technology, Beijing 100190, People's Republic of China*
[9]*China University of Geosciences, Wuhan 430074, People's Republic of China*
[10]*Chung-Ang University, Seoul, 06974, Republic of Korea*
[11]*COMSATS University Islamabad, Lahore Campus, Defence Road, Off Raiwind Road, 54000 Lahore, Pakistan*
[12]*Fudan University, Shanghai 200433, People's Republic of China*
[13]*GSI Helmholtzcentre for Heavy Ion Research GmbH, D-64291 Darmstadt, Germany*
[14]*Guangxi Normal University, Guilin 541004, People's Republic of China*
[15]*Guangxi University, Nanning 530004, People's Republic of China*
[16]*Hangzhou Normal University, Hangzhou 310036, People's Republic of China*
[17]*Hebei University, Baoding 071002, People's Republic of China*
[18]*Helmholtz Institute Mainz, Staudinger Weg 18, D-55099 Mainz, Germany*
[19]*Henan Normal University, Xinxiang 453007, People's Republic of China*
[20]*Henan University, Kaifeng 475004, People's Republic of China*
[21]*Henan University of Science and Technology, Luoyang 471003, People's Republic of China*
[22]*Henan University of Technology, Zhengzhou 450001, People's Republic of China*
[23]*Huangshan College, Huangshan 245000, People's Republic of China*
[24]*Hunan Normal University, Changsha 410081, People's Republic of China*

[25]*Hunan University, Changsha 410082, People's Republic of China*
[26]*Indian Institute of Technology Madras, Chennai 600036, India*
[27]*Indiana University, Bloomington, Indiana 47405, USA*
[28a]*INFN Laboratori Nazionali di Frascati, I-00044 Frascati, Italy*
[28b]*INFN Sezione di Perugia, I-06100, Perugia, Italy*
[28c]*University of Perugia, I-06100 Perugia, Italy*
[29a]*INFN Sezione di Ferrara, I-44122 Ferrara, Italy*
[29b]*University of Ferrara, I-44122 Ferrara, Italy*
[30]*Inner Mongolia University, Hohhot 010021, People's Republic of China*
[31]*Institute of Modern Physics, Lanzhou 730000, People's Republic of China*
[32]*Institute of Physics and Technology, Peace Avenue 54B, Ulaanbaatar 13330, Mongolia*
[33]*Instituto de Alta Investigación, Universidad de Tarapacá, Casilla 7D, Arica 1000000, Chile*
[34]*Jilin University, Changchun 130012, People's Republic of China*
[35]*Johannes Gutenberg University of Mainz, Johann-Joachim-Becher-Weg 45, D-55099 Mainz, Germany*
[36]*Joint Institute for Nuclear Research, 141980 Dubna, Moscow region, Russia*
[37]*Justus-Liebig-Universitaet Giessen, II. Physikalisches Institut,*
Heinrich-Buff-Ring 16, D-35392 Giessen, Germany
[38]*Lanzhou University, Lanzhou 730000, People's Republic of China*
[39]*Liaoning Normal University, Dalian 116029, People's Republic of China*
[40]*Liaoning University, Shenyang 110036, People's Republic of China*
[41]*Nanjing Normal University, Nanjing 210023, People's Republic of China*
[42]*Nanjing University, Nanjing 210093, People's Republic of China*
[43]*Nankai University, Tianjin 300071, People's Republic of China*
[44]*National Centre for Nuclear Research, Warsaw 02-093, Poland*
[45]*North China Electric Power University, Beijing 102206, People's Republic of China*
[46]*Peking University, Beijing 100871, People's Republic of China*
[47]*Qufu Normal University, Qufu 273165, People's Republic of China*
[48]*Renmin University of China, Beijing 100872, People's Republic of China*
[49]*Shandong Normal University, Jinan 250014, People's Republic of China*
[50]*Shandong University, Jinan 250100, People's Republic of China*
[51]*Shanghai Jiao Tong University, Shanghai 200240, People's Republic of China*
[52]*Shanxi Normal University, Linfen 041004, People's Republic of China*
[53]*Shanxi University, Taiyuan 030006, People's Republic of China*
[54]*Sichuan University, Chengdu 610064, People's Republic of China*
[55]*Soochow University, Suzhou 215006, People's Republic of China*
[56]*South China Normal University, Guangzhou 510006, People's Republic of China*
[57]*Southeast University, Nanjing 211100, People's Republic of China*
[58]*State Key Laboratory of Particle Detection and Electronics, Beijing 100049,*
Hefei 230026, People's Republic of China
[59]*Sun Yat-Sen University, Guangzhou 510275, People's Republic of China*
[60]*Suranaree University of Technology, University Avenue 111, Nakhon Ratchasima 30000, Thailand*
[61]*Tsinghua University, Beijing 100084, People's Republic of China*
[62a]*Turkish Accelerator Center Particle Factory Group, Istinye University, 34010, Istanbul, Turkey*
[62b]*Near East University, Nicosia, North Cyprus, 99138, Mersin 10, Turkey*
[63]*University of Chinese Academy of Sciences, Beijing 100049, People's Republic of China*
[64]*University of Groningen, NL-9747 AA Groningen, The Netherlands*
[65]*University of Hawaii, Honolulu, Hawaii 96822, USA*
[66]*University of Jinan, Jinan 250022, People's Republic of China*
[67]*University of Manchester, Oxford Road, Manchester M13 9PL, United Kingdom*
[68]*University of Muenster, Wilhelm-Klemm-Strasse 9, 48149 Muenster, Germany*
[69]*University of Oxford, Keble Road, Oxford OX13RH, United Kingdom*
[70]*University of Science and Technology Liaoning, Anshan 114051, People's Republic of China*
[71]*University of Science and Technology of China, Hefei 230026, People's Republic of China*
[72]*University of South China, Hengyang 421001, People's Republic of China*
[73]*University of the Punjab, Lahore-54590, Pakistan*
[74a]*University of Turin and INFN, University of Turin, I-10125 Turin, Italy*
[74b]*University of Eastern Piedmont, I-15121, Alessandria, Italy*
[74c]*INFN, I-10125 Turin, Italy*
[75]*Uppsala University, Box 516, SE-75120 Uppsala, Sweden*
[76]*Wuhan University, Wuhan 430072, People's Republic of China*

[77]*Yantai University, Yantai 264005, People's Republic of China*
[78]*Yunnan University, Kunming 650500, People's Republic of China*
[79]*Zhejiang University, Hangzhou 310027, People's Republic of China*
[80]*Zhengzhou University, Zhengzhou 450001, People's Republic of China*

[a]Deceased.
[b]Also at the Moscow Institute of Physics and Technology, Moscow 141700, Russia.
[c]Also at the Novosibirsk State University, Novosibirsk 630090, Russia.
[d]Also at the NRC "Kurchatov Institute", PNPI, 188300 Gatchina, Russia.
[e]Also at Goethe University Frankfurt, 60323 Frankfurt am Main, Germany.
[f]Also at Key Laboratory for Particle Physics, Astrophysics and Cosmology, Ministry of Education; Shanghai Key Laboratory for
Particle Physics and Cosmology; Institute of Nuclear and Particle Physics, Shanghai 200240, People's Republic of China.
[g]Also at Key Laboratory of Nuclear Physics and Ion-beam Application (MOE) and Institute of Modern Physics, Fudan University,
Shanghai 200443, People's Republic of China.
[h]Also at State Key Laboratory of Nuclear Physics and Technology, Peking University, Beijing 100871, People's Republic of China.
[i]Also at School of Physics and Electronics, Hunan University, Changsha 410082, China.
[j]Also at Guangdong Provincial Key Laboratory of Nuclear Science, Institute of Quantum Matter, South China Normal University,
Guangzhou 510006, China.
[k]Also at MOE Frontiers Science Center for Rare Isotopes, Lanzhou University, Lanzhou 730000, People's Republic of China.
[l]Also at Lanzhou Center for Theoretical Physics, Lanzhou University, Lanzhou 730000, People's Republic of China.
[m]Also at the Department of Mathematical Sciences, IBA, Karachi 75270, Pakistan.
[n]Also at Ecole Polytechnique Federale de Lausanne (EPFL), CH-1015 Lausanne, Switzerland.
[o]Also at Helmholtz Institute Mainz, Staudinger Weg 18, D-55099 Mainz, Germany.